ERDC/TN DOER-I7
May 2019

Bubble Image Velocimetry with an Acoustic Camera

by David L. Young, Brian C. McFall, and Duncan B. Bryant

PURPOSE: This Dredging Operations and Environmental Research (DOER) Technical Note (TN) describes the equipment and techniques necessary to perform bubble image velocimetry (BIV) using images acquired from an acoustic camera (*imaging sonar*).

BACKGROUND: BIV is a subset of particle image velocimetry (PIV), a common laboratory experimental technique used to measure flow velocity. In traditional particle image velocimetry, the flow of interest is seeded with tracer particles that reflect light and are assumed to faithfully follow the motion of the fluid, which is a valid assumption with sufficiently small particles (Adrian and Westerweel 2011). In BIV, bubbles are used in place of tracer particles (Ryu et al. 2005). In either case, the motion of the tracer particles/bubbles is observed—generally with a charge-coupled device or complementary metal-oxide semiconductor digital camera for modern systems—and used to quantify the flow velocity. The flow velocity is measured by sub-dividing the camera images into windows (e.g., 16 × 16 pixels); then, cross-correlation is used to determine the aggregate displacement of all the particles in each window between successive images (Raffel et al. 2007). However, traditional PIV and BIV measurement techniques with an optical camera are difficult to deploy in the field because they are equipment intensive, require stationary, well-calibrated images, and can only be performed in a reasonably transparent fluid (such that the optical camera can see the tracer particles/bubbles). Obviously these requirements quickly become restrictive in field deployments, particularly in highly turbid environments near dredging operations.

In this document, a procedure is described to acquire the images and perform the analysis for planar PIV-style measurements with an acoustic camera rather than the traditional optical camera. Acoustic cameras, or imaging sonars, are small multi-beam active sonars that transmit sound pulses into the region of interest and use the returning sound to reconstruct a digital image (Young et al. 2017). Use of an acoustic camera addresses the turbid water issue and partially addresses the extensive equipment requirements that have proven problematic for field deployment of PIV-style measurement techniques (Young and McFall 2017). Acoustic cameras can easily operate in turbid environments with low optical clarity (Belcher et al. 2001; Kim et al. 2005; Belcher 2006; Wu et al. 2008). Additionally, the acoustic camera performs the primary functions of both the illumination source and the camera in a traditional PIV/BIV system by both emitting and receiving acoustic waves. This significantly lessens the size and power requirements that have proven prohibitive to performing PIV/BIV in the field. Finally, the acoustic camera images do not require extensive calibration to convert pixel space to physical space, as required with optical camera images. That information can be directly gleaned from the acoustic waves transmitted and received by the acoustic camera. The range to the object(s) scattering the emitted acoustic waves is determined by the time elapsed between the emission of

Approved for public release; distribution is unlimited.

the acoustic wave and the return of the sound scattered by the object (Urick 1983). The direction relative to the camera position is determined by *beamforming* (or *spatial filtering*)—using the observed lag between adjacent transducers observing the same sound returning to the transducer array (van Veen and Buckley 1988).

EQUIPMENT AND DATA AQUISITION: The acoustic camera used in this study was a Sound Metrics ARIS 3000 Explorer Imaging Sonar (Figure 1 - Sound Metrics Corp., Bellevue, WA) with an operating frequency of 3 megahertz. The camera possesses 128 beams (sound emitting and receiving transducers), each emitted at a slightly different angle such that collectively they span the entire width of the camera viewing window (30º in-plane spreading angle). Each beam measures the intensity of the returned sound at a series of 600 bins, equidistantly spaced from the camera blanking distance (70 centimeters [cm] from the camera) to the specified maximum range of the camera. For the data presented in this study, the user-set minimum and maximum camera ranges were 124 and 284 cm, respectively.

Figure 1. Picture of a Sound Metrics ARIS 3000 Imaging Sonar. (Sound Metrics Corp. Bellevue, Washington. Re-printed from www.soundmetrics.com with permission.)

The camera was equipped with a 1º concentrator lens, which reduces the out-of-plane spreading angle of the acoustic camera to 1º (from a standard spreading angle of 14º) without altering the operating frequency of the camera. This focuses the acoustic energy into a narrower volume, increasing the resolution of the images, allowing smaller particles/bubbles to be observed, and forcing the insonified volume to better mimic a thin plane—as required for planar PIV analysis. The maximum obtainable framerate of the Sound Metrics acoustic camera was 15 frames per second (fps). The acoustic camera was chosen based on the following considerations: (1) the out-of-plane concentrator lens is critical to perform planar PIV-style analysis. If the out-of-plane spreading angle cannot be restricted, then the camera is unsuitable for PIV-style analysis; (2) cameras with higher operating frequencies result in higher resolution images at the cost of

reduced maximum range (Urick 1983); (3) all else being equal, cameras with a larger number of beams and bins will return higher resolution images, assuming the in-plane spreading angles are similar.

The flow measured in this study was the canonical velocity field in the wake of a circular cylinder. Images of the flow in the wake of the cylinder were collected for 5 minutes at the maximum framerate of 15 fps, resulting in 4,500 total images. The images were collected with Sound Metrics software used to control the camera (Ariscope) and saved as a proprietary filetype (.aris). An image of the flow output from the software accompanying the acoustic camera is shown in Figure 2. The little blue dots liberally scattered throughout the image are micro-bubbles suspended in the flow that are visible to the acoustic camera. Bubbles are highly visible in acoustic-camera images because the acoustic impedance of air is substantially lower than that of water (Kinsler et al. 2000). Consequently, if bubbles are present in the flow in significant quantities and are sufficiently small, they make excellent tracers for PIV-style analysis with an acoustic camera. As the number and size distribution of the bubbles in the flow are critical, bubble size and quantity were directly measured with a Dynaflow Acoustic Bubble Spectrometer (ABS - Dynaflow, Inc., Jessup, MD). The ABS determines the bubble population by making acoustic measurements at several frequencies with a pair (or several pairs) of hydrophones. The bubble population is then determined by the solution to two Fredholm Integral Equations of the first kind (Wu et al. 2014).

Note that an acoustic camera requires a completely different viewing position than an optical camera to observe (ostensibly) the same image. As shown in Figure 3, optical cameras are generally placed to observe the image in a position perpendicular to the image plane. In contrast, for the authors' purposes the acoustic camera must be placed to view *along* the plane of the image. Finally, as PIV-style measurements with an acoustic camera are still very much an experimental technique, it is recommended to validate any such measurements with a more commonly accepted measurement technique (optical PIV, acoustic Doppler velocimeters [ADVs], acoustic Doppler current profilers, etc.).

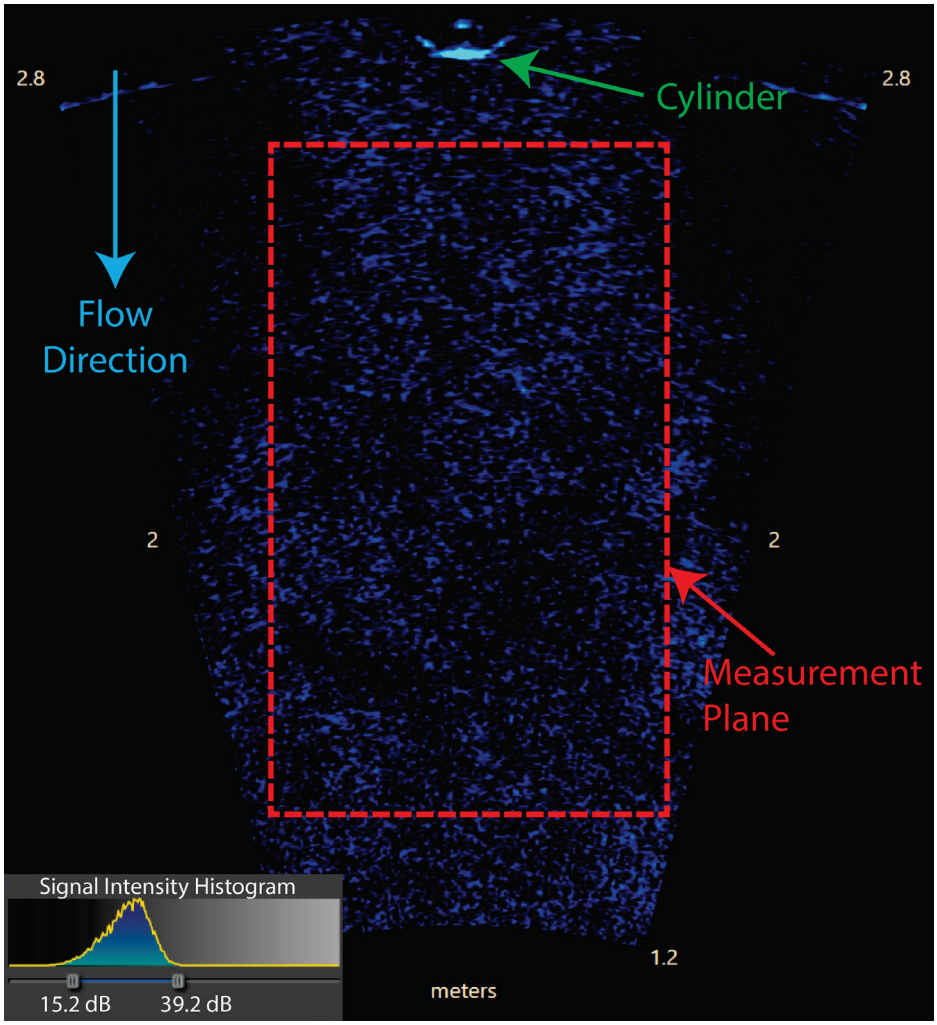

Figure 2. Image of the flow downstream of a cylinder from the acoustic camera. Units displayed to either side are distance away from the camera.

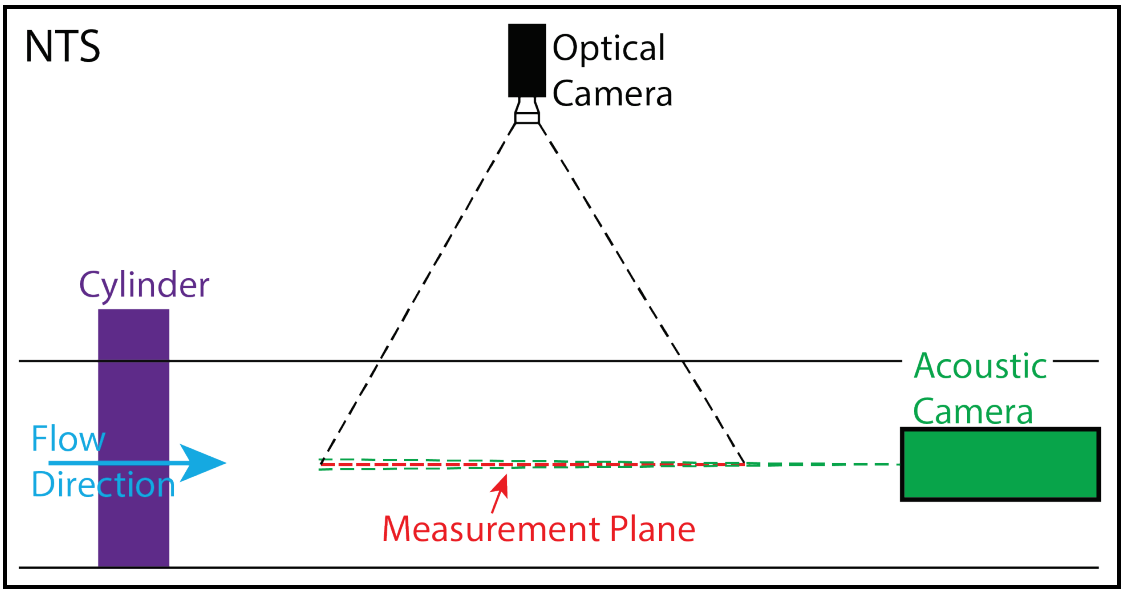

Figure 3. Viewing angle of an acoustic camera compared with an optical camera.

DATA PROCESSING: Raw data from the acoustic camera were extracted from the proprietary acoustic camera movie file-type (.aris) using custom *arisreader.m* functions developed in Matlab (Mathworks, Inc., Natick, MA). These functions produce the intensity of the returned sound at every bin within each camera beam in machine units (0 - 255). The machine units correspond linearly to the measurable range of intensities of the sound returned to the acoustic camera in decibels (dB) (0 – 80 dB for the acoustic camera used in this study).

Data Filtering. As only the raw data can be extracted from the .aris, the data filtering algorithms available in the Sound Metrics software must be recreated in Matlab to achieve the same quality images as those displayed in the software (and in Figure 2). Specifically, two data processing algorithms to filter the raw acoustic camera data were deployed. First is a minimum and maximum dB threshold algorithm. This filter is done because the signal from the bubbles visible in the acoustic camera images typically occupies a comparatively narrow band of the full dB range of the camera. For example, based on the signal intensity histogram for the data collection observed in Figure 2 (see bottom left corner of Figure 2), the bubbles are primarily observed in the range 15.2 – 39.2 dB. To isolate the bubbles, all bins in which the observed intensity is less than the minimum of the allowable intensity range (15.2 dB) are set to zero. Then, all bins in which the observed intensity is greater than the maximum of the allowable intensity range (39.2 dB) are set to the value of the maximum of the intensity range. Finally, the intensity in all of the bins is scaled up such that the maximum intensity observed prior to the filter is the same as the maximum intensity observed after the filter has been applied.

The second data processing algorithm used to filter the raw acoustic camera data is a mean signal intensity subtraction. This filter subtracts the average bin intensity across time from each bin. After this filter is applied, the intensity in all of the bins is scaled back up to the maximum intensity observed prior to the filter application. Any remaining bins with observed intensity less than 0 dB are set to 0 dB. This filter has the effect of removing any static parts of the resulting movie, as the intensity in those bins is constant with time.

Polar Data to Cartesian Images. By their very nature, the acoustic camera data are in polar coordinates; thus, the sample size of each bin increases linearly with distance away from the camera. For the data presented in this study, the minimum and maximum areas of the bins were 14 mm^2 and 37 mm^2, respectively, with an average area of 25 mm^2. Using simple trigonometry, the angle of each beam relative to the camera axis, and the distance from the acoustic camera to the sample bin, it is possible to reconstruct a Cartesian image from the filtered polar coordinate data. This procedure was performed using a custom Matlab script written with guidance from Sound Metrics. As a consequence of the polar-to-Cartesian conversion, the *resolution* of the Cartesian image must be manually specified rather than directly determined by the pixel resolution of the imaging sensor (as would be the case for an image acquired with a digital camera). To ensure adequate Cartesian image reconstruction, each pixel in the Cartesian images used in this study was set to correspond to a 1.5 mm × 1.5 mm square, resulting in images that became progressively more oversampled with distance away from the acoustic camera. The Cartesian image from each frame of the acoustic camera movie was written to a .bmp file by the Matlab script. An example of two reconstructed Cartesian images, one without and one with filtering, is displayed in Figure 4. Notice the reduction in background noise, sharpening of the tracer bubbles, and the removal of the stationary cylinder in the filtered image.

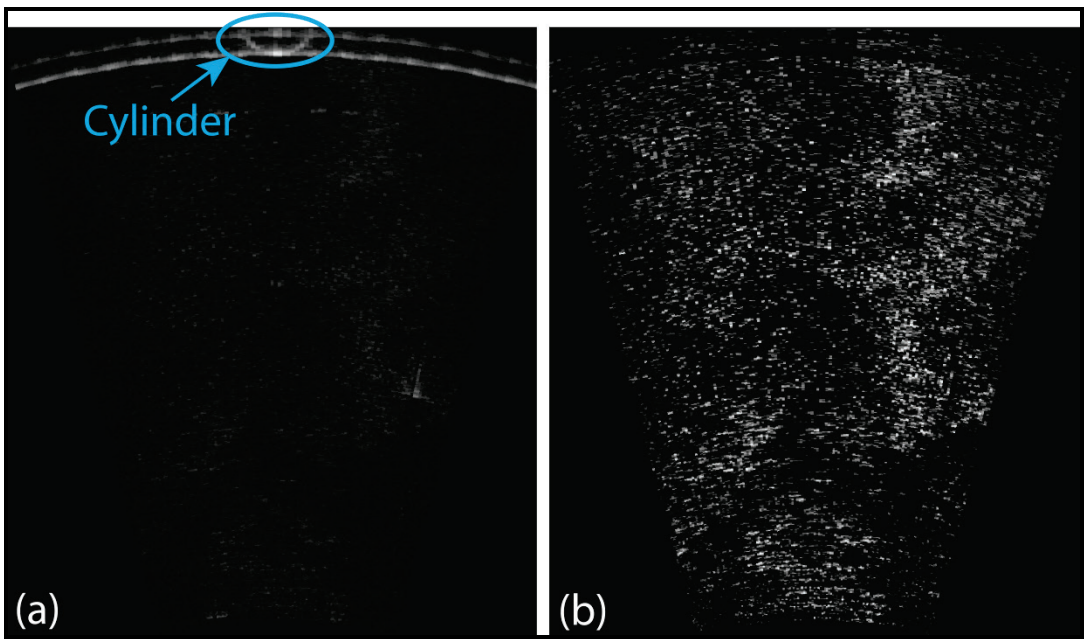

Figure 4. (a) Unfiltered and (b) filtered Cartesian images generated from raw acoustic camera data.

PIV Processing. Once the filtered images were written out, the process proceeded in the same manner as traditional planar PIV analysis. The .bmp files were loaded into PIV processing software to obtain velocity vectors. The velocity data presented in this study were obtained via cross-correlation with a window size of 32 × 32 pixels using the commercially available PIV software DaVis (LaVision, Ypsilanti, MI), but alternatives are available (e.g., mpiv in Matlab - Mori and Chang 2003). To ensure adequate pixel displacement of the tracer bubbles between

frames, every third image was used in the PIV processing. A total of 1,454 instantaneous velocity vector fields were written out to .dat files for analysis.

SAMPLE RESULTS: The concept of using an acoustic camera to conduct BIV measurements was examined using the canonical flow past a cylinder. This experiment was conducted in a 1.98 meter (m)-wide flume located at the U.S. Army Engineer Research and Development Center in Vicksburg, MS. The flume was 14 m long, and the 19 cm diameter cylinder was placed on the flume centerline 10.25 m from the flow straightener at the head of the flume. Notably, there was a mildly sloped section 190 cm upstream of the cylinder where the bed drops 6 cm over 117 cm. The flowrate for this data was 0.04 m^3 per second (m^3/s), corresponding to an average velocity of 5 cm/s and Re_D of 9400, given the flume dimensions. A diagram of the experimental setup is shown in Figure 5. The velocity results from the acoustic camera BIV were benchmarked against an array of five Nortek Vectrino ADVs. Data were collected by the ADVs at three distinct cross sections spaced 20 cm apart in the downstream direction, beginning 32 cm downstream of the cylinder. The ADVs were spaced 18 cm apart. Two sets of ADV measurements were made at each cross section; one in the original configuration and one with the array of ADVs translated 9 cm in the cross-stream direction. Thus, each cross section consisted of 10 sets of ADV measurements spaced 9 cm apart.

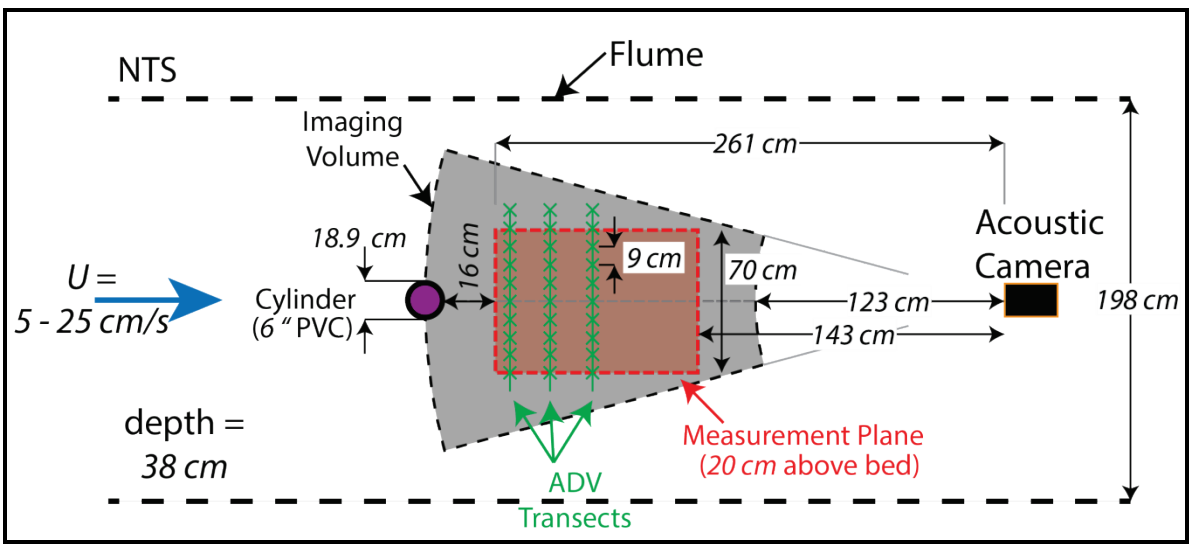

Figure 5. Diagram of the experimental setup.

As the ADV and acoustic camera results were not time synced, only statistical flow characteristics were compared, specifically the mean downstream velocity (U in Figure 6) and the standard deviations of the cross-stream and downstream velocities (σ_v in Figure 7 and σ_u in Figure 8, respectively). Velocities were normalized by the maximum mean velocity observed in the acoustic camera BIV data (U_{max}) and distances were normalized by the cylinder diameter (D). To determine if the periodic shedding of vortices in the cylinder wake was detected, the power spectral densities (PSDs) of the cross-stream velocity between the ADV and the acoustic camera at (x/D = 2.82, y/D = 1.14) were compared in Figure 9 alongside the shedding frequency estimated by the Strouhal number ($St = f_{Sr}D/U = 0.20$). The PSD is an estimate of the energy in the signal (the downstream or cross-stream velocities) at a series of discrete frequencies. The PSDs are plotted on log-log axes.

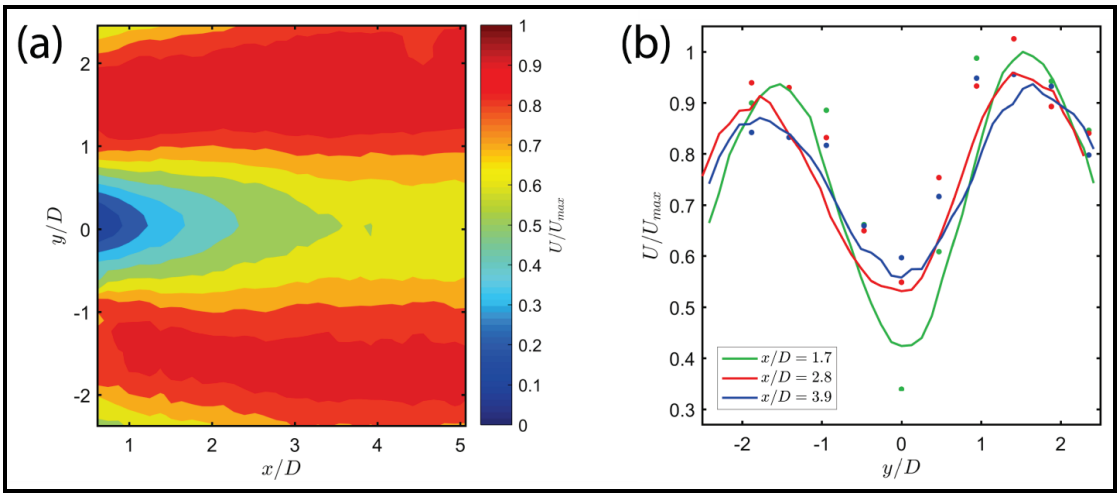

Figure 6. (a) Mean downstream velocity (U) from the acoustic camera and (b) comparison of mean downstream velocity between ADV cross sections (dots) and acoustic camera cross sections (lines).

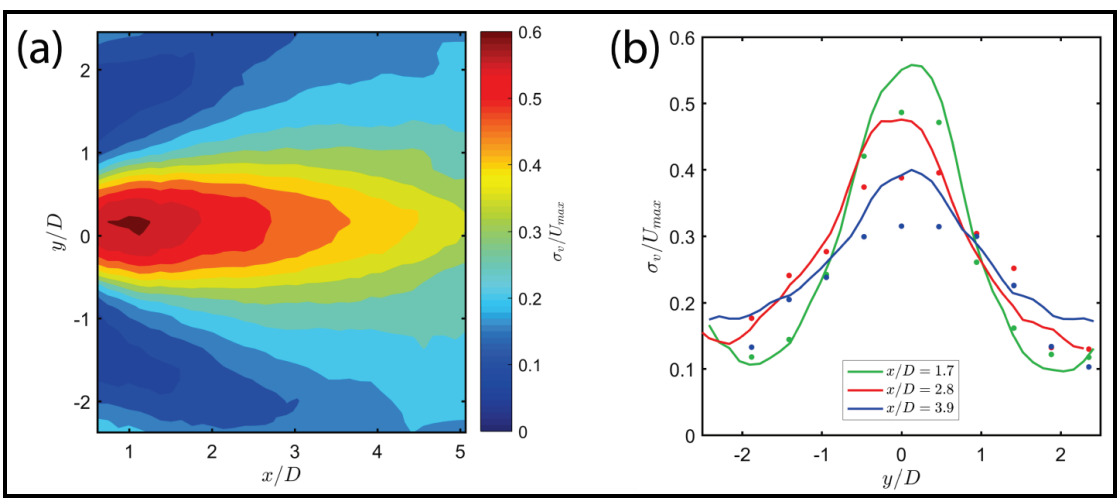

Figure 7. (a) Standard deviation of cross-stream velocity (σ_v) from the acoustic camera and (b) comparison of standard deviation of cross-stream velocity between ADV cross sections (dots) and acoustic camera cross sections (lines).

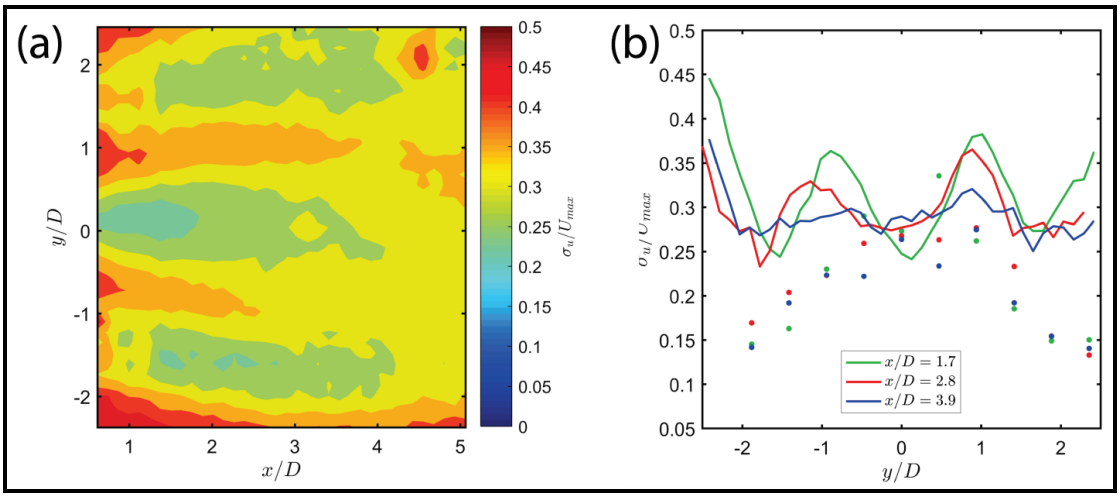

Figure 8. (a) Standard deviation of downstream velocity (σ_u) from the acoustic camera and (b) comparison of standard deviation of downstream velocity between ADV cross sections (dots) and acoustic camera cross sections (lines).

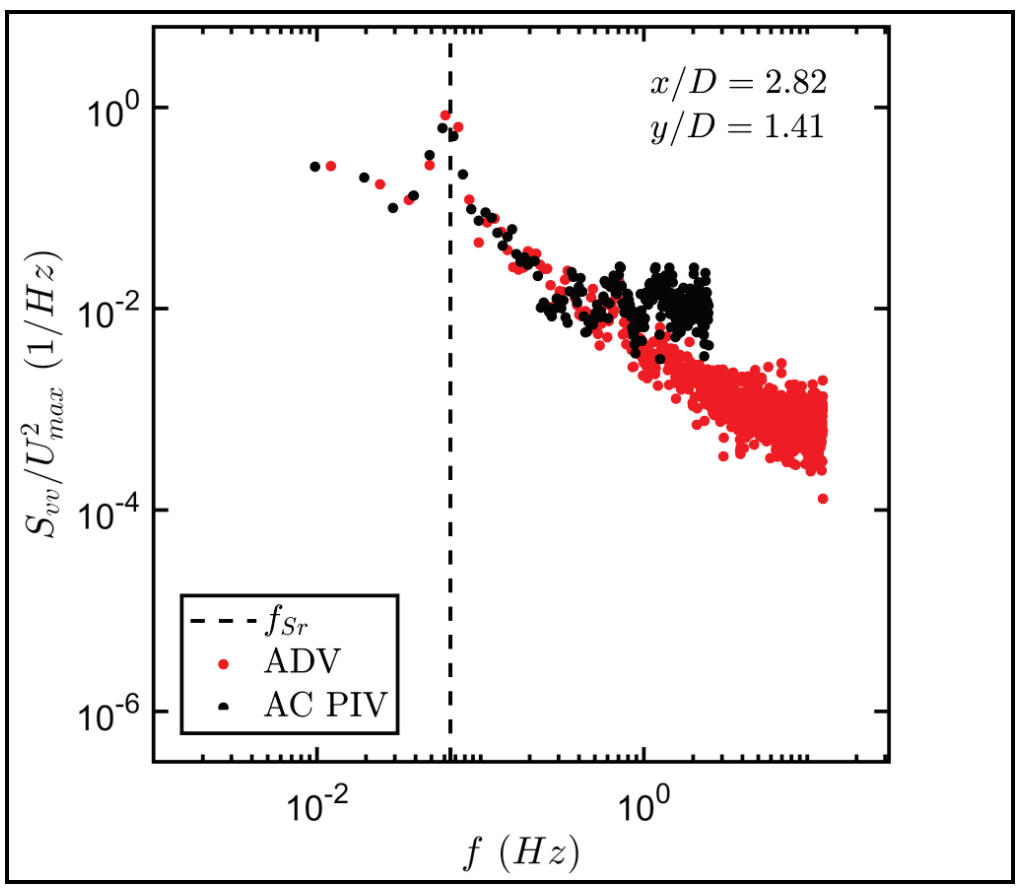

Figure 9. Comparison of the PSDs of the cross-stream velocity at (x/D = 2.82, y/D = 1.41) from the acoustic camera (black dots) and the ADV (red dots). The shedding frequency of the vortices in the wake of the cylinder based on the Strouhal number (f_{Sr}) is plotted as a dashed black line.

The acoustic camera slightly undermeasures the magnitude of the cross-stream variability in the mean downstream velocity (Figure 6) but returns the proper profile shape and profile evolution in the wake of the cylinder. Additionally, the acoustic camera slightly overmeasures the magnitude of the standard deviation of the cross-stream velocity (Figure 7), yet again the appropriate profile shape and downstream evolution were captured. The acoustic camera does not accurately reproduce the standard deviation of the downstream velocity (Figure 8). The profile shape was distinctly different than that expected in the wake of the cylinder (i.e., greater at the edges rather than at the center). This suggested a zero-mean source of noise at the periphery of the viewing window as the bubbles approached the acoustic camera (i.e., downstream) that was not accounted for in the filtering of this study. Finally, the signal from the vortex shedding was detected in both the ADV and the acoustic camera (Figure 9), with local spikes in both PSDs centered on the estimated vortex shedding frequency (f_{Sr}).

SUMMARY AND FUTURE DEVELOPMENT: This study describes in detail the materials and methods necessary to perform BIV using images obtained from an acoustic camera. When compared to measurements made from ADVs, the acoustic camera slightly under- and overmeasures the magnitudes of the cross-stream variability in the mean downstream velocities and the cross-stream velocity fluctuations, respectively, but displays the correct profile shapes. The nature of the errors indicates they may be rectified by further calibration. However, there was significant error in the downstream velocity fluctuations, suggesting a source of noise at the periphery of the viewing window present as the bubbles approach the acoustic camera. Future work will entail further refining the technique and image processing algorithms to improve the acoustic camera measurements and more rigorous testing of the conditions under which the acoustic camera images are of sufficient quality to perform the BIV analysis.

ADDITIONAL INFORMATION: This Dredging Operations and Environmental Research (DOER) Technical Note (TN) was prepared as part of the U.S. Army Corps of Engineers (USACE) DOER Program by Drs. David L. Young, Brian C. McFall, and Duncan B. Bryant, U.S. Army Engineer Research and Development Center (ERDC), Coastal and Hydraulics Laboratory (CHL). Questions pertaining to this CHETN may be directed to Dr. David L. Young (*david.l.young@usace.army.mil*) or to the USACE DOER Program Manager, Dr. Todd S. Bridges (*todd.s.bridges@usace.army.mil*).

This ERDC/TN DOER-I7 should be cited as follows:

> Young, D. L., B. C. McFall, and D. B. Bryant. 2019. *Bubble Image Velocimetry with an Acoustic Camera.* ERDC/TN DOER-I7. Vicksburg, MS: U.S. Army Engineer Research and Development Center. *http://dx.doi.org/10.21079/11681/32863*

REFERENCES

Adrian, R. J., and J. Westerweel. 2011. *Particle Image Velocimetry*. Cambridge Aerospace Series No. 30. New York: Cambridge University Press.

Belcher, E. O. 2006. Acoustic camera produces near-video quality images. *Sea Technology* 47(12):27–31.

Belcher, E. O., B. Matsuyama, and G. M. Trimble. 2001. Object identification with acoustic lenses. In *OCEANS 2001, MTS/IEEE Conference and Exhibition*. Vol. 1, 6–11. IEEE. doi:10.1109/oceans.2001.968656.

Kim, K., N. Neretti, and N. Intrator. 2005. Mosaicing of acoustic camera images. In *IEE Proceedings – Radar, Sonar and Navigation.* 152(4): 263–270. doi:10.1049/ip-rsn:20045015.

Kinsler, L., A. Frey, A. Coppens, and J. Sanders. 2000. *Fundamentals of Acoustics,* 4th edition. New York: John Wiley and Sons, Inc.

Mori, N., and K. A. Chang. 2003. An experimental study of a horizontal jet in a wavy environment. *ASCE Journal of Engineering Mechanics* 129(10):1149–1155. doi:10.1061/(ASCE)0733-9399(2003)129:10(1149).

Raffel, M., C. Willert, S. Wereley, and J. Kompenhans. 2007. *Particle Image Velocimetry: A Practical Guide.* 2nd edition. Berlin: Springer-Verlag.

Ryu, Y., K.-A. Chang, and H. J. Lim. 2005. Use of bubble image velocimetry for measurement of plunging wave impinging on a structure and associated greenwater. *Measurement Science and Technology* 16(10):1945–1953. http://dx.doi.org/10.1088/0957-0233/16/10/009.

Urick, R. J. 1983. *Principles of Underwater Sound.* 3rd edition. New York: McGraw-Hill.

van Veen, B. D., and K. M. Buckley. 1988. Beamforming: a versatile approach to spatial filtering. *IEEE ASSP Magazine* 5(2):4–24. doi:10.1109/53.665.

Wu, F.-C., Y.-C. Shao, C.-K. Wang, and J. Liou. 2008. Potential for application of an acoustic camera in particle tracking velocimetry. *Review of Scientific Instruments* 79(11):116102-1–116102-3. http://dx.doi.org/10.1063/1.3021046.

Wu, X., M. Wendall, G. L. Chahine, and B. Riemer. 2014. Gas bubble size measurements in liquid mercury using an acoustic spectrometer. *ASME Journal of Fluids Engineering* 136(3):031303-1–031303-9.

Young, D. L., and B. C. McFall. 2017. *The Feasibility of Performing Particle-Tracking-Based Flow Measurements with Acoustic Cameras*. ERDC/CHL SR-17-1. Vicksburg, MS: U.S. Army Engineer Research and Development Center.

Young, D. L., B. C. McFall, T. L. Welp, and D. D. Dickerson. 2017. Use of acoustic cameras in dredging research. In *2017 Dredging Summit & Expo Proceedings,* 164–175. Vancouver, British Columbia, Canada.

NOTE: *The contents of this technical note are not to be used for advertising, publication, or promotional purposes. Citation of trade names does not constitute an official endorsement or approval of the use of such products.*